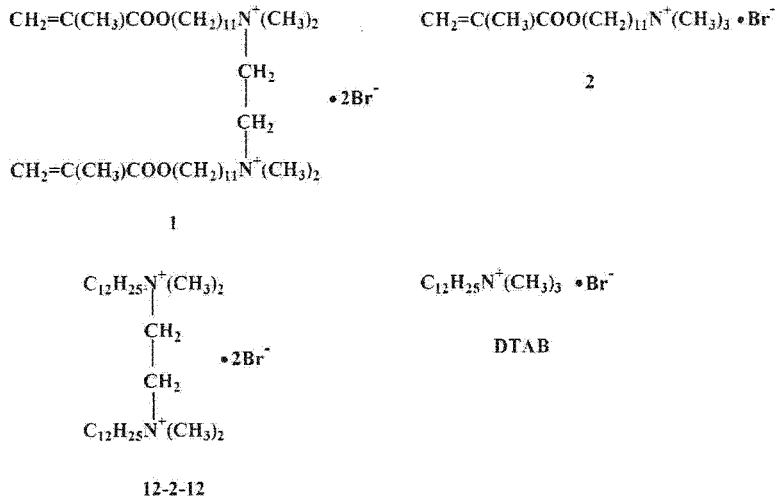

Figure 1. Chemical structures of polymerizable cationic gemini surfactant, **1**, the corresponding monomer, **2**, cationic gemini surfactant, 12−2−12, and the corresponding monomer, DTAB.

Scheme 1. Synthetic Route for Polymerizable Cationic Gemini Surfactant

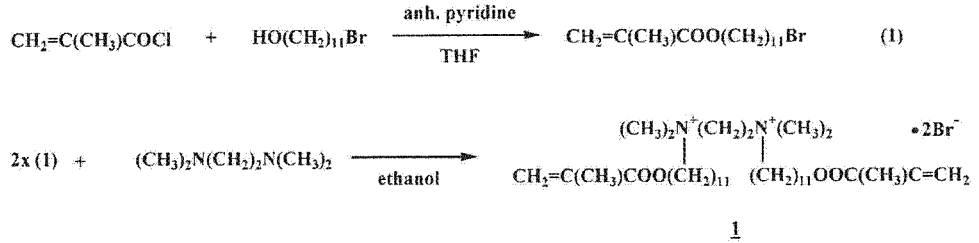

ammonium bromide), 12−2−12[14-16] and DTAB,[1c] which is a monomer corresponding to 12−2−12.

Materials and Methods

Materials. The polymerizable cationic gemini surfactant, $CH_2{=}C(CH_3)COO(CH_2)_{11}N^+(CH_3)_2(CH_2)_2N^+(CH_3)_2(CH_2)_{11}$-$OOC(CH_3){=}CH_2{\cdot}2Br^-$, **1**, was synthesized according to Scheme 1. The reagents and solvents used were 11-bromo-1-undecanol (98%), *N,N,N′,N′*-tetramethylethylenediamine (99.5%), 2,2′-azobis(2-methylpropionamidine) dihydrochlolide (97%) (all from Aldrich), methacryloyl chloride (97%), anhydrous pyridine (99.8%), and THF (99.9%) (all from Tokyo Chemical Industry). Bromoundecyl methacrylate was synthesized by the reaction of 11-bromo-1-undecanol with methacryloyl chloride in the presence of 4-methoxyphenol and anhydrous pyridine in THF according to the usual method.[13,17] The polymerizable cationic gemini surfactant, **1**, was synthesized as follows. The mixture of *N,N,N′,N′*-tetramethylethylenediamine (2.1 g, 0.018 mol), bromoundecyl methacrylate (13.1 g, 0.038 mol), 4-methoxyphenol (0.13 g), and anhydrous ethyl alcohol (50 mL) was stirred at 80 °C for 48 h. The solvent was evaporated off under reduced pressure. The residue obtained was purified by column chromatography on a silica gel column using chloroform/methanol (5:2, v/v) as a mobile phase. The polymerizable gemini surfactant, **1**, as a white solid was obtained (10.8 g, 80% yield, mp 139.9 °C). ^{1}H NMR ($CDCl_3$) δ1.21−1.38 (br, 32H), 1.63−1.79 (m, 8H), 1.94 (s, 6H), 3.42−3.51 (br, 12H), 3.69−3.75 (t, 4H), 4.11−4.15 (t, 4H), 4.76 (s, 4H), 5.55 (s, 2H), 6.10 (s, 2H) ppm; ^{13}C NMR ($CDCl_3$) δ167.43, 136.30, 125.12, 65.78, 64.60, 56.54, 50.90, 29.26−29.02 (m), 28.40, 26.09, 25.75, 22.88, 18.19 ppm; FAB-MS (*m/z*,): 673, 675 $(M\text{-}Br)^-$; Anal. Found: C, 57.20; H, 9.53; N, 3.93%. Calcd. for $C_{36}H_{70}N_2$: C, 57.45; H, 9.31; N, 3.72%. The chemical purity checked by two-phase titration method is 97%. The polymerizable monomeric surfactant, **2**, was synthesized by the reaction of bromoundecyl methacrylate with trimethylamine in the presence of 4-methoxyphenol according to the usual method.[13,17] The analytical data are as follows: ^{1}H NMR ($CDCl_3$): δ1.28−1.36 (br, 14H), 1.62−1.78 (m, 4H), 1.94 (s, 3H), 3.42−3.51 (br, 9H), 3.56−3.61 (t, 2H), 4.11−4.16 (t, 4H), 5.55 (s, 1H), 6.10 (s, 1H) ppm; ^{13}C NMR ($CDCl_3$) δ167.29, 136.19, 124.95, 66.57, 64.51, 53.08, 29.09−28.88 (m), 28.28, 25.87−25.64 (m), 22.92, 18.06 ppm; Anal. Found: C, 57.23; H, 9.89; N, 3.66%. Calcd. for $C_{18}H_{36}N$: C, 57.14; H, 9.58; N, 3.70%. The chemical purity checked by two-phase titration method is 95%, mp 117.4 °C. Tetradecyltrimethylammonium bromide (TTAB) and cetyltrimethylammonium bromide (CTAB) from Tokyo Chemical Industry were recrystallized 5 times before use ($CHCl_3$/ethyl alcohol mixture).

Surface Tension Measurements. The surface tensions were measured with Wilhelmy plate technique (surface tensiometer CBVP-Z, Kyowa Kaimenkagaku Co., Ltd., Japan). Measurements were taken at 30 ± 0.1 °C until constant surface tension values indicated that equilibrium with an experimental error within 0.1 mN/m had been reached. The cmc values were taken at the intersection of the linear portions of the plots of the surface tension against the logarithm of the surfactant concentration. Solutions were prepared with ultrapure water (30 L Diamond Storage Reservoir, Barnstead International, U. S.A). NaBr was baked in a porcelain casserole at 500 °C.

Transmission Electron Microscopy (TEM). Transmission electron micrographs were obtained using a standard tungsten filament-type TEM (H-7650, Hitachi Science Systems, Ltd.) operated at an accelerating voltage of 120 kV. A small amount of sample solution was placed on the surface of a TEM copper grid covered by a holey carbon film and dried under vacuum for 1 day. The TEM grid was then observed directly in the TEM. Images were recorded digitally by a CCD camera equipped in the TEM.

(14) Achouri, M. E.; Infante, M. R.; Izquierdo, F.; Kertit, S.; Gouttya, H. M.; Nerdi, B. *Corroision Sci.* **2001**, *43*, 19.
(15) Atkin, R.; Craig, V. S. J.; Wanless, E. J.; Biggs, S. *J. Phys. Chem. B* 2003, *107*, 2978.
(16) Pisarcik, M.; Rosen, M. J.; Polakovicova, M.; Devinsky, F.; Lacko, I. *J. Colloid Interface Sci.* **2005**, *289*, 560.
(17) Summers, M. J.; Eastoe, J.; Davis, S. A.; Du. Z.; Richardson, R. M.; Heenan, R. K.; Steytler, D.; Grillo, I. *Langmuir* **2001**, *17*, 5388.

Table 1. Surface Properties of All Surfactants Investigated and the Related Surfactants

surfactant	media	cmc (M)	γ_{cmc} (mN/m)	pC_{20}	A_{min} (10^2nm^2)	$\Gamma_{max} \times 10^{10}$ (mol/cm^2)	cmc/C_{20}
1	water	5.0×10^{-4}	32.1	4.8	220	0.7	30
12−2−12[14,15,16]	water	8.4×10^{-4a}	32[a]	4.8[a]			
2	water	1.8×10^{-2}	42.1	2.3	129	1.3	4.0
DTAB[1c,19]	water	1.6×10^{-2a}	39[a]	2.1[a]	2.4		
TTAB	water	3.7×10^{-3}	37.8	2.9	63	2.6	2.8
CTAB	water	9.0×10^{-4}	37.6	3.7	73	2.3	3.3
1	0.05 M NaBr	4.0×10^{-5}	27.8	6.0	63	2.6	40
2	0.05 M NaBr	1.3×10^{-2}	41.7	2.8	90	1.9	8.2
TTAB	0.05 M NaBr	5.1×10^{-4}	35.2	4.1	47	3.5	6.4
CTAB	0.05 M NaBr	6.2×10^{-5}	33.1	5.1	48	3.4	7.3

[a] 25 °C.

Micelle Size Measurements. Micelle size distribution was determined by the dynamic light scattering method at 30 ± 0.1 °C with a NICOMP380 ZLS (Particle Sizing System Co., U.S.A.). Measurements were continued up to a constant micelle size distribution values with an experimental error within 1%.

Results and Discussion

Figure 1 shows the plots of surface tension (γ) vs log molar surfactant concentration (log C) at 30 °C for **1**, **2**, TTAB, and CTAB in water and in 0.05 M NaBr solution. Saturation adsorption values, Γ_{max}, at the air/water interface and values of minimum area per molecule, A_{min}, were calculated using the Gibbs equation[1d]

$$\Gamma_{max} = \frac{-1}{2.303nRT}\left(\frac{\partial\gamma}{\partial \log C}\right)_T \quad (1)$$

$$A_{min} = (N_A\Gamma_{max})^{-1} \times 10^{16} \quad (2)$$

where γ is the surface tension in mN/m, T is the absolute temperature, $R = 8.31$ J/(mol K), and N_A is Avogadoro's number. Γ_{max} and A_{min} are expressed in mol/cm^2 and in $10^2 \times$ nm^2/molecule, respectively. The value of n in the Gibbs equation is the number of ionic species whose concentration at the interface varies with change in the surfactant concentration in the solution. In the absence of added electrolyte in aqueous solution, the value of n for ionic surfactants decreases with increase in the surfactant concentration, since this increase causes changes in the counterion concentration. For divalent gemini surfactants, $n = 3$ (the gemini amphiphile species and the two counterions).[18,19,21] Since the surfactant concentrations for the Γ_{max} calculation in water (below the cmc) were all at <0.018 molar concentrations, we can assume no significant effect change in the surfactant concentration on the ionic strength of the solution. However, in the presence of 0.05 M NaBr, there is no change in the counterion concentration in the aqueous solution and consequently at the interface with a change in the concentration of surfactant; therefore, $n = 1$.[19−24] Table 1 lists the values of cmc, γ_{cmc}, pC_{20} (−log C_{20}), Γ_{max}, and A_{min} in water for all surfactants, together with some reference values of cationic surfactants, 12−2−12[14−16] and DTAB.[1c] The values of A_{min} in the absence of added electrolyte, in Table 1, are based upon $n = 3$ for **1** and $n = 2$ for the monomeric surfactants, respectively. The cmc values of TTAB and CTAB in water are in good accordance with literature values.[1c,19] It is apparent from the data in Table 1 that **1** has cmc values 2 orders of magnitude smaller and a C_{20} value (the surfactant concentration required to reduce the surface tension of the solvent by 20 mN/m, shown in Table 1 as the pC_{20} value, the negative log of the C_{20} value) 2 or 3 order of magnitude smaller than that for **2**. This is in agreement with previous work[18−21] showing that the presence of two hydrophobic groups in the gemini molecule results in greater surface activity. The values of γ_{cmc}, 32.1 mN/m, and pC_{20}, 4.8, in water of **1** are equal to 32 mN/m[14] and 4.78,[14] of 12−2−12, respectively (see Table 1), meaning that a methacryloxyundecyl group is equivalent to 12 CH_2 groups in adsorbed film formation. On the other hand, the γ_{cmc} value in water, 42.1 mN/m, of **2** is larger than that, 39.0 mN/m[1c], of DTAB. The pC_{20} value in water, 2.3, of **2** is also larger than that, 2.1[1c], of DTAB. The reason for these behaviors is discussed below. Additionally, the $-CO{\cdot}OCH_2CH_2-(CH_2)_9-$ group is equivalent to 10.27 CH_2 groups since the ester group $-CO{\cdot}OCH_2CH_2-$ is equivalent to 1.27 CH_2 groups.[23] This means that the influence of the $CH_2{=}C(CH_3)-$ group is equal to 1.7 CH_2 groups. The larger cmc/C_{20} ratio for **1** than **2** indicates that the gemini surfactants have a greater preference to be adsorbed at the air/water interface relative to their preference to form micelles than the monomeric surfactant.[1b] This is due to the steric inhibition of convex micelle formation by the two hydrophobic groups of the gemini surfactant.[22] Note that the cmc/C_{20} ratio for **2**, having a methachryloyl group in a terminal hydrophobic group, is larger than those of conventional monomeric surfactants, DTAB, TTAB, and CTAB. One explanation is some steric factor inhibiting micellization relative adsorption.[1b,21,22,24] The larger A_{min} value of **2** than those for the conventional cationic surfactants, TTAB and CTAB, is in agreement with this hypothesis.

Table 1 also lists the values of cmc, γ_{cmc}, pC_{20} (−log C_{20}), Γ_{max}, and A_{min} in 0.05 M NaBr. In this case, the value of the coefficient in the Gibbs adsorption equation to calculate the value of A_{min} is one. Because of the low solubility just below the cmc the gemini surfactant, **1**, shows no break in the γ vs log C plots at 30 °C in 0.1 M NaBr solution. The values of cmc, γ_{cmc}, pC_{20}, Γ_{max}, and A_{min} of **1** are comparable in both water and 0.05 M NaBr. The polymerizable cationic gemini surfactant, **1**, and the polymerizable cationic monomeric surfactant, **2**, have apparently a lower γ_{cmc} value, a larger pC_{20} value, and a larger Γ_{max} value (and consequently smaller A_{min} value) in 0.05 M NaBr than in water due to increased ionic strength and shielding effect of electrolyte ions which promote increased aggregation in the volume and denser packing of surfactant monomers at the interface which results in decreasing γ_{cmc}.[1d,17−20,22] The γ_{cmc} values of surfactants reflects their cmc/C_{20} ratio and A_{min} according to[1e]

$$\pi_{cmc} = \gamma_0 - \gamma_{cmc} = 20 + nRT\Gamma_{max} \ln(\text{cmc}/C_{20}) \quad (3)$$

Therefore, the γ_{cmc} values involve both the cmc/C_{20} ratios and the A_{min} (or Γ_{max}) values. From the cmc, Γ_{max}, and pC_{20} (−log

(18) Tajima, K.; Imai, Y.; Nakamura, A.; Tsubone, K.; Mimura, K.; Nakatsuji, Y.; Ikeda, I. *J. Oleo Sci.* **2001**, *50*, 453.
(19) Rosen, M. J.; Mathias, J. H.; Davenport, L. *Langmuir* **1999**, *15*, 7340.
(20) Song, L. D.; Rosen, M. J. *Langmuir* **1996**, *12*, 1149.
(21) Tsubone, K.; Arakawa, Y.; Rosen, M. J. *J. Colloid Interface Sci.* **2003**, *262*, 516.
(22) Li, F.; Rosen, M. J.; Sulthana, S. B. *Langmuir* **2001**, *17*, 1037.
(23) Devinsky, F.; Masarova, L.; Lacko, I. *J. Colloid Interface Sci.* **1985**, *105*, 236.
(24) Tsubone, K.; Rosen, M. J. *J. Colloid Interface Sci.* **2001**, *244*, 394.

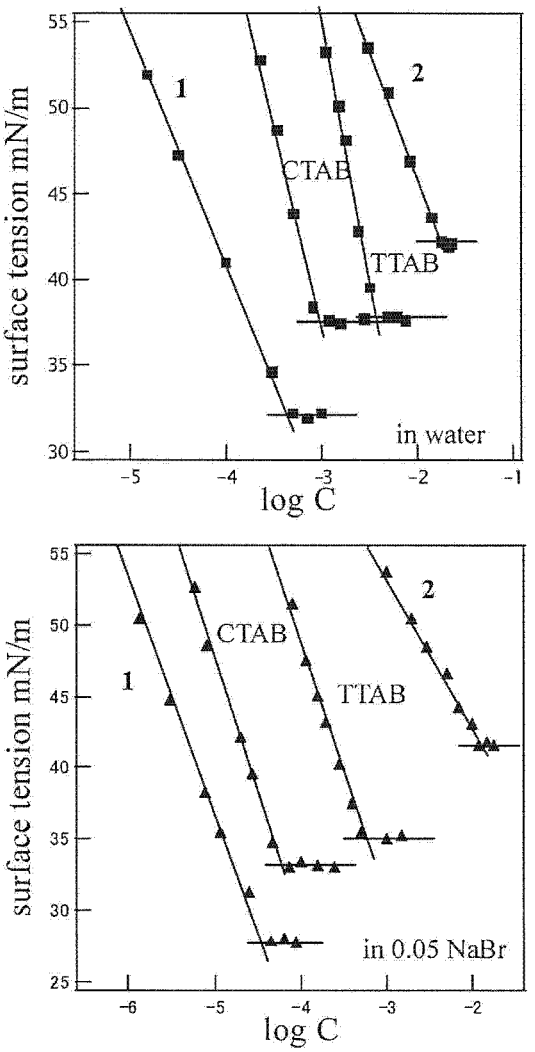

Figure 2. Surface tension vs log C plots in water and 0.05 M NaBr for all surfactants used.

C_{20}) values in 0.05 M NaBr in Table 1, the decreasing order of Γ_{max} ln(cmc/C_{20}) for surfactants investigated is **1** > CTAB > TTAB > **2**, and this order corresponds to the order of increasing γ_{cmc}. The finding that the larger A_{min} value of the polymerizable cationic monomeric surfactant, **2**, than those for the conventional cationic surfactants observed in water was also true in the salt solution to give an additional evidence for the hypothesis mentioned above. The terminal location of the methacryloxy group in a molecule of **2** is favorable to have a loop-like conformation that the dipolar terminal group can optimize the weak interaction with water molecules at the air/water interface as suggested by Hamid et al.[13] Hence, the molecules of **2** lie at the interface in such a way that oxygen atoms in a methacryloxy group are in contact with the interface to form bolaform-type amphiphile[25-27] such as $R_3N^+-(CH_2)_n-N^+R_3$ type cationic surfactants[26] and ferrocenyl surfactants [27] that have the structure $Fc(CH_2)_nN^+(CH_3)_3Br^-$, where Fc is a ferrocene group. The higher cmc value in water of **2** than that of DTAB is attributable to this bolaform-type conformation at the solution/micelle interface.

(25) Nagarajan, R. *Chem. Eng. Commun.* **1987**, *55*, 251.
(26) Menger, F. M.; Wrenn, S. *J. Phys. Chem.* **1974**, *78*, 1387.
(27) Abbott, N. L. *Stud. Surf. Sci. Catal.* **2001**, *132*, 49.

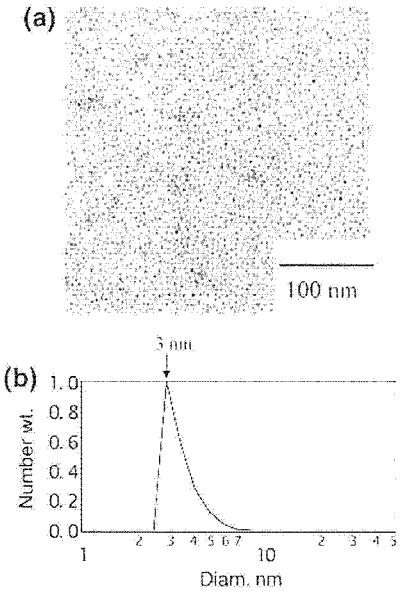

Figure 3. TEM image of polymerized micelles of cationic gemini surfactant, **1**, and their size of distribution.

Noteworthy is the finding that the A_{min} value of the polymerizable cationic gemini surfactant, **1**, is significantly smaller than that of the corresponding monomeric surfactant, **2**. In general, the A_{min} value of the gemini surfactants is smaller than double the A_{min} value for the corresponding monomeric surfactants because the hydrophobic groups of the former can pack more closely in adsorbed film at the air/water interface than those in the latter.[18-22] The smaller A_{min} value of **1** than that of **2** in 0.05 M NaBr strongly suggests that molecules of the polymerizable cationic gemini surfactant, **1**, have no conformation of bolaform-type amphiphile at the air/water interface (no-loop conformation). The γ_{cmc} (or pC_{20}) value in water of **1** is equal to that of 12−2−12, whereas the γ_{cmc} (or pC_{20}) value in water of **2** is larger (smaller) than that of DTAB, yielding additional evidence for the no-loop conformation of **1**.

Polymerization of gemini surfactant **1** was performed at its concentration of 20 mM in water at 60 °C for 2 h in a sealed vial using a water-soluble free radical initiator, 2,2′-azobis(2-methylpropionamidine) dihydrochlolide at a concentration of 0.2 mM. The appearance of the sample obtained was almost unchanged visually and kept its clearness after polymerization even at room temperature though the sample viscosity increased. The process of polymerization was monitored by checking the diminution of vinyl signals in the ^{1}H NMR spectrum of a sample solution prepared in D_2O. The completion of polymerization was confirmed by the disappearance of vinyl protons signals in the NMR spectrum. Figure 3a is a TEM image of the polymerized micelles in water after 20-fold dilution of the sample, showing fairly small monodisperse, spherical particles with a mean diameter of about 3 nm (Figure 3b). The micelle size distribution was determined by the dynamic light scattering method. An important point to be noted is that the micelle size thus obtained is smaller than 5 nm, the value for **2**.[3] The smaller size of the polymerized micelles of **1** than those of the polymerized micelles of **2** is not surprising, and we are encouraged to prepare nanostructural and spherical architectures with a high surface area in a near future.

In summary, we have synthesized a polymerizable cationic gemini surfactant having a methacryloxy group at the terminal of undecyl group and two methylene groups as a spacer in a

molecule, **1**, and investigated its interfacial properties in water and in 0.05 M NaBr. For comparison, the properties of the corresponding monomer, **2**, a cationic gemini surfactant, 12−2−12, and the conventional cationic surfactant, DTAB, TTAB, and CTAB, were also investigated. The results obtained are as follows: (1) The unexpected smaller A_{min} value of **1** than that of **2** in 0.05 M NaCl suggests that the gemini surfactant molecules, **1**, have no bolaform-type conformation at the air/water interface, whereas the corresponding monomeric surfactants molecules have this type of conformation. (2) The γ_{cmc} (or pC_{20}) value in water of **1** is equal to that of 12−2−12, whereas the γ_{cmc} (or pC_{20}) value in water of **2** is larger (smaller) than that of DTAB, yielding additional evidence for the no-loop conformation of **1** in adsorption film formation. (3) The polymerized micelles of the gemini surfactant are fairly small monodisperse, and spherical particles with a mean diameter of 3 nm.

LA060156Y

PO Box 2345, Beijing 100023, China
www.wjgnet.com
wjg@wjgnet.com

World J Gastroenterol 2007 February 14; 13(6): 821-825
World Journal of Gastroenterology ISSN 1007-9327

EDITORIAL

The hepatic sinusoidal endothelial lining and colorectal liver metastases

Filip Braet, Keissuke Nagatsuma, Masaya Saito, Lilian Soon, Eddie Wisse, Tomokazu Matsuura

Filip Braet, Lilian Soon, Eddie Wisse, Australian Key Centre for Microscopy and Microanalysis, Electron Microscopy Unit, The University of Sydney, NSW 2006, Australia
Keissuke Nagatsuma, Department of Pathology, The Jikei University School of Medicine, Tokyo, Japan
Masaya Saito, Division of Gastroenterology and Hepatology, Department of Internal Medicine, The Jikei University School of Medicine, Tokyo, Japan
Tomokazu Matsuura, Department of Laboratory Medicine, The Jikei University School of Medicine, Tokyo, Japan
Correspondence to: A/Professor Filip Braet, Australian Key Centre for Microscopy and Microanalysis, Electron Microscope Unit, Madsen Building F09, University of Sydney, Sydney, NSW 2006, Australia. filip.braet@emu.usyd.edu.au
Telephone: +61-2-93517619 Fax: +61-2-93517682
Received: 2006-11-08 Accepted: 2006-12-21

Abstract

Colorectal cancer (CRC) is a common malignant disease and the severe nature of cases in men and women who develop colorectal cancer makes this an important socio-economic health issue. Major challenges such as understanding and modeling colorectal cancer pathways rely on our understanding of simple models such as outlined in this paper. We discuss that the development of novel standardized approaches of multidimensional (correlative) biomolecular microscopy methods facilitates the collection of (sub) cellular tissue information in the early onset of colorectal liver metastasis and that this approach will be crucial in designing new effective strategies for CRC treatment. The application of X-ray micro-computed tomography and its potential in correlative imaging of the liver vasculature will be discussed.

Key words: Apoptosis; Australia; Correlative microscopy; Endothelial cells; Hepatic metastasis; Colorectal cancer; CC531; Gaps; Interferon gamma; Kupffer cells; Natural killer cells; Nitric oxide; Macrophages; Modeling; Phagocytosis; Plugging; Pit cells; Stellate cells; X-ray micro-computed tomography

Braet F, Nagatsuma K, Saito M, Soon L, Wisse E, Matsuura T. The hepatic sinusoidal endothelial lining and colorectal liver metastases. *World J Gastroenterol* 2007; 13(6): 821-825

http://www.wjgnet.com/1007-9327/13/821.asp

INTRODUCTION

Colorectal cancer (CRC) is a common malignant disease, with the majority of deaths attributable to hepatic metastasis. In the Western world, it is the second cause of cancer death in women after breast cancer, and the third cause of cancer death in men after lung and prostate cancer, being responsible for about 492 000 deaths p.a. worldwide and 4500 deaths p.a. in Australia[1]. In addition, the statistical data reveal that the risk of developing CRC disproportionately strikes individuals in the age group 65 years and older, illustrating its health longevity impact on the ageing population. At the first diagnosis of CRC, 20% of the patients already have liver metastasis and 30% of the patients will develop metastasis afterwards. 80% of the patients who die of CRC have metastases in the liver and prognosis is generally poor[2].

It is obvious that once the tumour cells have immigrated to the liver, they cross the hepatic sinusoidal endothelial barrier and by the time liver metastases form, most steps in the metastatic cascade have been completed. Consequently, exploring the preceding stages of CRC metastasis, proliferation and new blood vessel formation as well as mechanisms to disturb cell survival are to date of main interest as they are largely unexplored. As discussed in the following sections, the availability of new reconstructing and modeling techniques provide liver cancer biologists with an invaluable tool to bridge the gap between bench science and the development of potential novel liver CRC (immuno) therapeutic strategies.

COLORECTAL CANCER AND THE HEPATIC SINUSOIDAL IMMUNE SYSTEM

When the tumour cells invade the vascular bed and metastasise to the liver, they encounter the liver specific immune defence mechanisms. This hepatic sinusoidal immune system involves the hepatic-specific natural killer cells (NK) (pit cells)[3], Kupffer cells (KC) (liver-associated macrophages)[4] and hepatic endothelial cells (HEC)[5], and is proven to play an important role in protecting the liver from invading colon carcinoma cells[6]. The conventional paradigm of CRC liver metastasis is based on a multi-step process characterized by a series of structural, cellular and molecular events, which give the tumour cells the ability to proceed through the many phases of liver metastasis. Based on literature survey the following common sequence of key-events within the liver sinusoids are involved in the

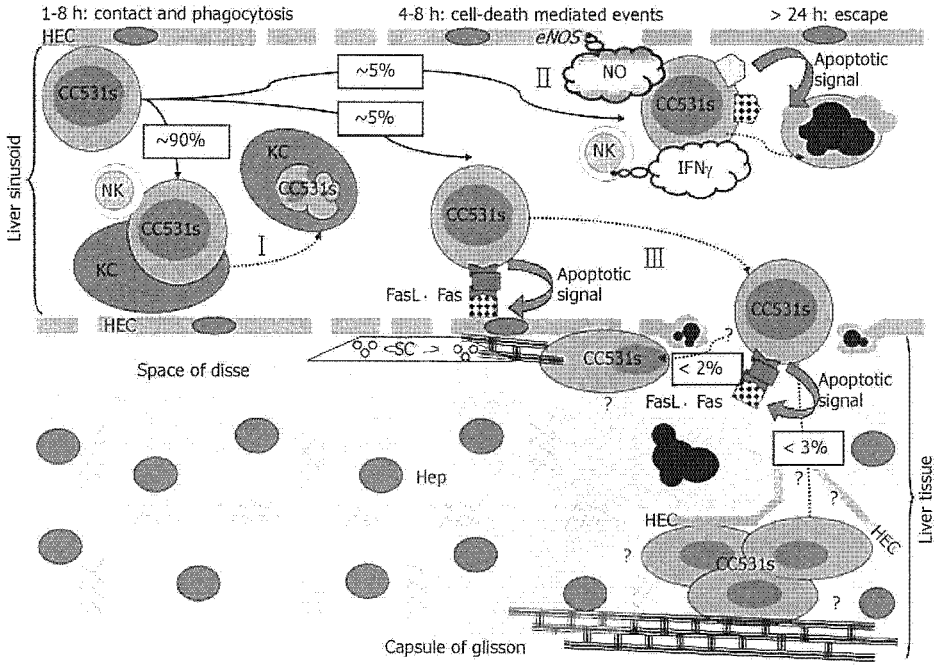

Figure 1 Schematic representation of the local hepatic sinusoidal immune defence system in the different steps of CRC liver metastasis (Steps I to III) as outlined in detail in the "*Phagocytosis, Apoptosis, Endothelial Retraction and Tumour Survival*"-section. The subsequent steps in the metastatic cascade as denoted by question marks illustrate that considerable work remains, especially once CRC cells traverse the sinusoidal endothelial lining and invade the liver tissue.

process of CRC liver metastasis: Tumour cells approach the liver tissue through finer branches of the portal vein, where they will be trapped in either the finest branch of the portal veins, or the portal hepatic sinusoids. These sinusoids are narrow and tortuous. The diameter of sinusoids is much smaller than the diameter of CRC cells. NK and KC are mobile cells and can be seen moving along the hepatic sinusoid in *in vivo* microscopy experiments (our unpublished data). At this stage, the NK and KC are seen to be associated with the majority of the tumour cells, resulting in cytolysis and subsequent phagocytosis of the majority of the cancer cells[7-9]. Subsequently, specific adhesion of tumour cells within the hepatic microcirculation and active extravasation of the surviving cancer cells through the damaged hepatic endothelium takes place[10]. Both are believed to be essential events for cancer metastasis in the liver[11]; although others postulate that tumour cells develop exclusively intravascularly during the early stages[12]. However, it has been demonstrated that endothelial damage and gap formation occurs in both scenarios, enabling large cellular surface interactions between the tumour cells and the hepatocytes[9-11].

In a later stage, matrix proteins derived from the stellate cells (SC) (liver-associated fibroblasts) are believed to provide a substrate for migration of tumour cells and infiltrating immuno-competent cells, whereas later on tight structures of matrix proteins surrounding tumour nodules provide a barrier for establishment of direct KC- and NK-cell-to-tumour-cell-contact and/or targeted therapies[9,13]. This is supported by the observation that large numbers of KC and NK cells were not activated at later phases in the metastasis process[14]. Finally, CRC cells spread throughout the liver, followed by the abdominal and peritoneal cavity[9,15].

PHAGOCYTOSIS, APOPTOSIS, ENDOTHELIAL RETRACTION AND TUMOUR SURVIVAL

Our previous microscopy and fine structural immunochemistry studies significantly contributed to the above model and as depicted in figure 1 we were able to demonstrate that KC, NK and HECs all work together in concert as one immune-surveillance guardian in the defence against CRC liver metastasis (Figure 1)[6]. Furthermore, it was shown that phagocytosis and apoptosis are key processes in three central steps in the complex CRC liver metastatic cascade, briefly: (Step I) When CC531s colon carcinoma cells encounter the liver sinusoid about 90% of the tumour cells are eliminated by a synergistic action between KC and NK cells[9]; (Step II) We have proven that HECs express FasL and that about 5% of the colorectal CC531s cell population express functional Fas under influence of IFNγ and NO released in the sinusoid by NK and HECs, respectively. In this situation, the IFNγ-activated pathway supports the immune system by inducing apoptosis in CC531s cells[16]; (Step III) Conversely, Fas expressing HEC undergo apoptosis by FasL expressing CC531s cells. As a result, about 5% of the CC531s cells are able to escape the local immune system and provide themselves a gateway towards the liver tissue as the HECs retracts. Next the CC531s cells have free access to the Fas expressing hepatocytes (Hep) which undergo in turn apoptosis by the FasL bearing CC531s cells and as a result invade the liver tissue[17]. Reconstruction data obtained *via* the aid of confocal laser scanning microscopy indicated that surviving cancer cells are primarily confined to the Space of Disse and to the Glisson capsule, suggesting that metastasis would initiate from this extracellular matrix-rich region.

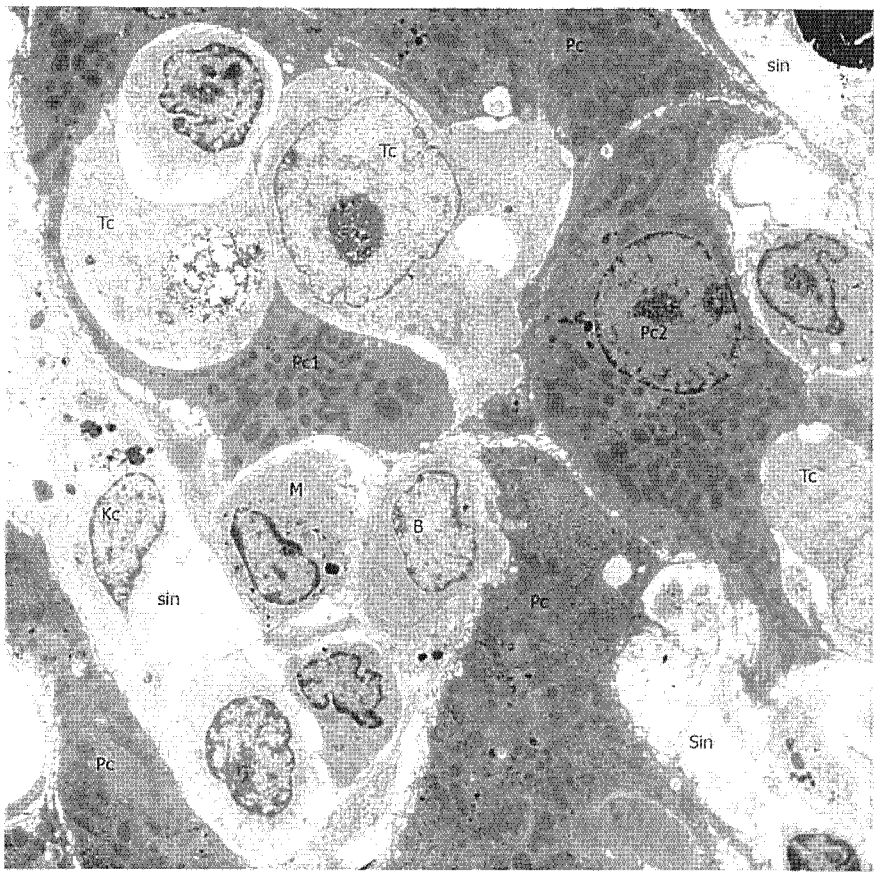

Figure 2 Transmission electron microscopy photomicrograph at low magnification (6700 x) of rat liver one week after i.v. injection of one million CC531s colon cancer cells. Tumour cells (Tc) can be recognized by a ribosome-rich, bulky cytoplasm containing few organelles. Tumour cell nuclei are large and contain mostly euchromatin. In this picture, tumour cells have already taken position in the liver parenchyma and compress or deform the parenchymal cells (Pc1 and Pc2). In this stage, tumour cells are so numerous that defending cells, such as Kupffer cells (Kc) and monocytes (M) in the hepatic sinusoids (Sin) and B lymphocytes (B) seem to be no longer involved as in earlier stages. At this stage of tumour cell settlement, rebuilding of the hepatic tissue sets in and soon small visible white spots of metastasis will be seen on the surface of the liver.

Overall, based on our combined light-, laser- and electron microscopic *in vivo* and *in situ* studies, we believe that the majority of tumour cells entering the liver will be destroyed in this first confrontation with hepatic sinusoidal cells. The trouble is supposed to be the fact that only a very few tumour cells need to escape from the hepatic sinusoids and after settling in the liver parenchymal tissue, as depicted in the photograph (Figure 2), they form metastases and start spreading new tumour cells in the hepatic tissue (i.e., secondary metastasis). It is also supposed that after leaving the hepatic sinusoids, the tumour cells are not chased by the local hepatic sinusoidal immune cells, and that the liver tissue has to rely from that moment onwards on other cellular- and immune defence systems, such as those offered by cytotoxic T cells, monocyte-derived macrophages and others.

RECONSTRUCTING AND MODELING COLORECTAL HEPATIC METASTASIS WITH CORRELATIVE THREE-DIMENSIONAL IMAGING TECHNIQUES

In the past, mainly two-dimensional structural tissue information has been generated about the metastasis pathways of CRC tumour formation in the liver. Attempts to target specific CRC pathways for therapeutic intervention, such as apoptosis by cell-death mediated drug delivery and/or new blood vessel outgrowth by specific anti-angiogenic drug release, partly failed because of our limited structural and molecular understanding about the tumour's complex cell- and tissue microenvironment using two-dimensional imaging. New concepts and progress in cell biology have been discovered thanks to improved correlative microscopy techniques that continue to rely predominantly on advances in new, three-dimensional (3D) reconstructing and modeling techniques[18,19]. Ideally, 3D correlative microscopy can be defined as an imaging platform aiming to cross-correlate information with multiple microscopy techniques on the same tissue(s) and/or cell(s). There is growing evidence from the literature that this approach facilitates the understanding of cellular and/or rare events by providing the possibility to collect new qualitative and quantitative information in a large sample volume[20,21]. In the past our group successfully applied different biomolecular microscopy methods on our CC531s CRC model. The data conferred under the above section were obtained by combining confocal laser scanning-[9,22], live cell-[23], atomic force-[24], scanning electron-[10,17] and transmission electron[16,25] microscopy data. In line, we started up correlative confocal laser scanning microscopy-[9,18] and X-ray micro-computed tomography (CT)[26] studies as defined above to quantitatively collect the spatial and temporal cell- and tissue architecture at different resolution levels of CRC hepatic metastasis (*vide infra*).

In a recent study[27], we applied the impregnation method in which en bloc staining of perfused-fixed hepatic tissue with osmium tetroxide and uranyl acetate was shown

to be successful to reconstruct and model a large sample volume of the macro- and microvasculature of hepatic tissue with X-ray micro-computed tomography (Figure 3). Furthermore, we demonstrated that correlative laser light optical imaging provided a limit of confidence for X-ray micro CT imaging of the hepatic vasculature as the large blood vessels such as the hepatic portal veins, and the smaller blood vessels i.e., the hepatic sinusoidal vascular bed could be visualized[27]. When applying the established contrasting method to the CC531s CRC metastasis model[9] it was observed that the dense array of blood vessels was interrupted in the liver tissue samples bearing the CRC cells when compared to the controls[27]. This is in line with the earlier observations made by Maehara[28] who showed tumour-induced reorganization of the auricular vascular bed after barium sulphate contrasting. Based on these data we forth casting the ability to correlate information in large tissue volumes from the X-ray micro CT models with reconstruction data obtained from confocal laser scanning microscopy on the same sample and region of interest by using fluorescent- and X-ray dense fiducial markers. This will definitely bridge the resolution gap from the micrometre to nanometre scale in studying cancer-mediated events, respectively.

In conclusion. Advanced multidimensional correlative microscopy methods and modeling techniques will feature heavily in the future quest to understand and to quantitatively define the spatial and temporal mechanisms regulating the pathways of CRC liver metastasis. There will be no doubt that elucidating the subcellular and molecular events of tumour-mediated cell-death processes (apoptosis) and collecting simultaneously additional structural and functional data in tumour-induced new blood vessel formation (angiogenesis) will be of main interest in future combined imaging studies as this approach will most probably result in an accurate correlative representation of the liver architecture and the tumour's microvasculature. One may hope that the combination of correlative insights gathered will be a breakthrough in the study of liver tumours and this will facilitate novel targeted cancer therapies in the long-term.

ACKNOWLEDGMENTS

The authors acknowledge the facilities as well as technical and administrative assistance from staff in the NANO Major National Research Facility at the "Australian Key Centre for Microscopy and Microanalysis" of The University of Sydney. T.M. and F.B. also acknowledge the support of the "Japan Association for the Advancement of Medical Equipment" (H17-nano-013 No. 141/Japanese Government-Ministry of Welfare and Labour). The authors are grateful to Ms. A. Simpson, Ms. E. Kable, Ms. E. Korkmaz & Dr. L. Cole, for excellent technical assistance, to Dr K. Vekemans for providing hepatic tissue (Figure 3A), and to Mr. G. Cohn, Mr. A. Restov & Dr. A. Jones for supporting Ms. S. Ananda and Ms. V. Marsden in soft X-ray imaging.

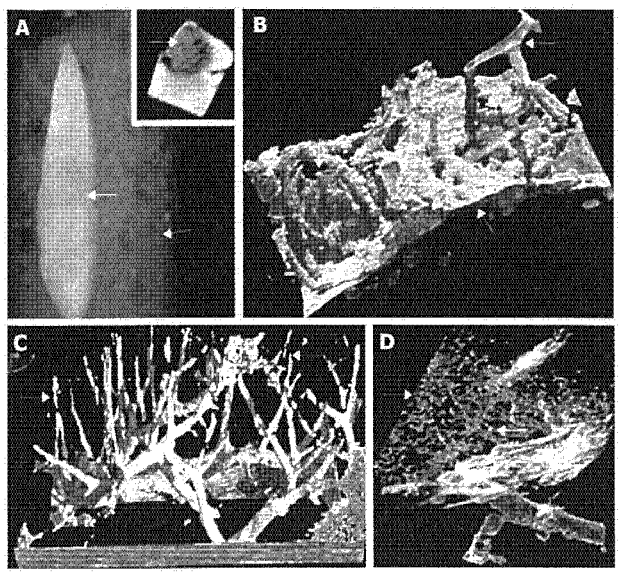

Figure 3 X-ray micro-computed tomography (CT) image set of hepatic tissue. For detailed recording and subsequent image processing settings we refer to Ananda *et al* (27). **A**: Low -magnification data showing an overview of a glutaraldehyde perfused-fixed and subsequently osmium tetroxide/uranyl acetate *en bloc* stained liver lobule (arrow) versus the unstained sample mounting support (arrowhead). Note, inset shows the corresponding Z-info at an ad random height of the main image; **B**: X-ray micro CT 3D reconstruction image showing the portal venous blood vessels (arrow) and hepatic tissue (arrowhead); **C**: X-ray micro CT reconstruction after density histogram image filtering, showing the intricate pattern of hepatic sinusoids (arrow) in 3D context. Note the absence of liver tissue information under this image processing condition (compare with B for the difference); **D**: Conversely, using different opacity thresholds resulted in the visualization of the hepatic cords, i.e. parenchymal tissue, (arrow). (Courtesy to Ms. S. Ananda and Ms. V. Marsden). Scale Bars (B-D), 500 μm.

COMMENTS

Background

Major challenges such as understanding and modeling colorectal liver metastases pathways rely on the understanding of simple models derived from large biomolecular image data sets.

Research frontiers

This paper elegantly demonstrated that the development of novel standardized approaches of multidimensional (correlative) biomolecular microscopy methods facilitated the collection of (sub) cellular tissue information in the early onset of colorectal liver metastasis and that this approach is crucial in designing new effective strategies for colorectal cancer treatment.

Innovations and breakthroughs

Advanced multidimensional correlative microscopy methods and modeling techniques will feature heavily in the future quest to understand and to quantitatively define the spatial and temporal mechanisms regulating the pathways of colorectal cancer liver metastasis.

Applications

There is no doubt that the "correlative insights"-approach, as discussed in depth in this "invitation expert review"-paper, will be a breakthrough in the study of liver tumours and will facilitate the design of novel targeted cancer therapies.

Terminology

Colorectal cancer is a common malignancy that frequently metastasizes to the liver. Identifying the mechanisms regulating the nanobiology of colorectal liver

metastasis, as well as gaining a better understanding of the interaction between the metastatic tumour cell and the different types of liver cells, including the liver vasculature, is a first when new therapeutic approaches wanted to be designed.

Peer review

How and why colorectal cancer cells metastasize to the liver has always been a subject of continuing interest. The authors describe this concept nicely, supported by excellent pictures.

REFERENCES

1 Australian Institute of Health and Welfare, Cancer in Australia 2000. Cancer series no. 23. Published 07-Nov-03; ISSN 1039-3307; ISBN 1-74024-328-5; AIHW Cat. no. CAN-18; ABS Cat, no. 8916.0

2 **Hamady ZZ**, Kotru A, Nishio H, Lodge JP. Current techniques and results of liver resection for colorectal liver metastases. *Br Med Bull* 2004; **70**: 87-104

3 **Nakatani K**, Kaneda K, Seki S, Nakajima Y. Pit cells as liver-associated natural killer cells: morphology and function. *Med Electron Microsc* 2004; **37**: 29-36

4 **Naito M**, Hasegawa G, Ebe Y, Yamamoto T. Differentiation and function of Kupffer cells. *Med Electron Microsc* 2004; **37**: 16-28

5 **Enomoto K**, Nishikawa Y, Omori Y, Tokairin T, Yoshida M, Ohi N, Nishimura T, Yamamoto Y, Li Q. Cell biology and pathology of liver sinusoidal endothelial cells. *Med Electron Microsc* 2004; **37**: 208-215

6 **Vekemans K**, Braet F. Structural and functional aspects of the liver and liver sinusoidal cells in relation to colon carcinoma metastasis. *World J Gastroenterol* 2005; **11**: 5095-5102

7 **Kan Z**, Ivancev K, Lunderquist A, McCuskey PA, McCuskey RS, Wallace S. In vivo microscopy of hepatic metastases: dynamic observation of tumor cell invasion and interaction with Kupffer cells. *Hepatology* 1995; **21**: 487-494

8 **Rushfeldt C**, Sveinbjornsson B, Seljelid R, Smedsrod B. Early events of hepatic metastasis formation in mice: role of Kupffer and NK-cells in natural and interferon-gamma-stimulated defense. *J Surg Res* 1999; **82**: 209-215

9 **Timmers M**, Vekemans K, Vermijlen D, Asosingh K, Kuppen P, Bouwens L, Wisse E, Braet F. Interactions between rat colon carcinoma cells and Kupffer cells during the onset of hepatic metastasis. *Int J Cancer* 2004; **112**: 793-802

10 **Vekemans K**, Timmers M, Vermijlen D, De Zanger R, Wisse E, Braet F. CC531s colon carcinoma cells induce apoptosis in rat hepatic endothelial cells by the Fas/FasL-mediated pathway. *Liver Int* 2003; **23**: 283-293

11 **Vidal-Vanaclocha F**. Role of sinusoidal endothelium in the pathogenesis of liver disease. In: Vidal-Vanaclocha F, editor. Functional Heterogeneity of Liver Tissue. Austin: R.G. Landes Company, 1997: 110-132

12 **Mook OR**, Van Marle J, Vreeling-Sindelarova H, Jonges R, Frederiks WM, Van Noorden CJ. Visualization of early events in tumor formation of eGFP-transfected rat colon cancer cells in liver. *Hepatology* 2003; **38**: 295-304

13 **Shimizu S**, Yamada N, Sawada T, Ikeda K, Kawada N, Seki S, Kaneda K, Hirakawa K. In vivo and in vitro interactions between human colon carcinoma cells and hepatic stellate cells. *Jpn J Cancer Res* 2000; **91**: 1285-1295

14 **Griffini P**, Smorenburg SM, Vogels IM, Tigchelaar W, Van Noorden CJ. Kupffer cells and pit cells are not effective in the defense against experimentally induced colon carcinoma metastasis in rat liver. *Clin Exp Metastasis* 1996; **14**: 367-80

15 **Lopes Cardozo AM**, Gupta A, Koppe MJ, Meijer S, van Leeuwen PA, Beelen RJ, Bleichrodt RP. Metastatic pattern of CC531 colon carcinoma cells in the abdominal cavity: an experimental model of peritoneal carcinomatosis in rats. *Eur J Surg Oncol* 2001; **27**: 359-363

16 **Vekemans K**, Braet F, Muyllaert D, Wisse E. Nitric oxide from rat liver sinusoidal endothelial cells induces apoptosis in IFN gamma-sensitized CC531s colon carcinoma cells. *J Hepatol* 2004; **41**: 11-18

17 **Vekemans K**, Braet F, Wisse E. DiO-labeled CC531s colon carcinoma cells traverse the hepatic sinusoidal endothelium via the Fas/FasL pathway. *J Gastrointest Surg* 2004; **8**: 371-372; author reply 372

18 **Robinson JM**, Takizawa T, Pombo A, Cook PR. Correlative fluorescence and electron microscopy on ultrathin cryosections: bridging the resolution gap. *J Histochem Cytochem* 2001; **49**: 803-808

19 **Grabenbauer M**, Geerts WJ, Fernadez-Rodriguez J, Hoenger A, Koster AJ, Nilsson T. Correlative microscopy and electron tomography of GFP through photooxidation. *Nat Methods* 2005; **2**: 857-862

20 **Koster AJ**, Klumperman J. Electron microscopy in cell biology: integrating structure and function. *Nat Rev Mol Cell Biol* 2003; **Suppl**: SS6-SS10

21 **Takizawa T**, Robinson JM. Correlative microscopy of ultrathin cryosections in placental research. *Methods Mol Med* 2006; **121**: 351-369

22 **Timmers M**, Vermijlen D, Vekemans K, De Zanger R, Wisse E, Braet F. Tracing DiO-labelled tumour cells in liver sections by confocal laser scanning microscopy. *J Microsc* 2002; **208**: 65-74

23 **Vekemans K**, Timmers M, Vermijlen D, Zanger RD, Wisse E, Braet F. Cytotoxic reactions of CC531s towards liver sinusoidal endothelial cells: a microscopical study. *Comp Hepatol* 2004; **3** Suppl 1: S49

24 **Braet F**, Vermijlen D, Bossuyt V, De Zanger R, Wisse E. Early detection of cytotoxic events between hepatic natural killer cells and colon carcinoma cells as probed with the atomic force microscope. *Ultramicroscopy* 2001; **89**: 263-73

25 **Vermijlen D**, Luo D, Froelich CJ, Medema JP, Kummer JA, Willems E, Braet F, Wisse E. Hepatic natural killer cells exclusively kill splenic/blood natural killer-resistant tumor cells by the perforin/granzyme pathway. *J Leukoc Biol* 2002; **72**: 668-676

26 **Ritman EL**. Micro-computed tomography-current status and developments. *Annu Rev Biomed Eng* 2004; **6**: 185-208

27 **Ananda S**, Marsden V, Vekemans K, Korkmaz E, Tsafnat N, Soon L, Jones A, Braet F. The visualization of hepatic vasculature by X-ray micro-computed tomography. *J Electron Microsc* (Tokyo) 2006; **55**: 151-155

28 **Maehara N**. Experimental microcomputed tomography study of the 3D microangioarchitecture of tumors. *Eur Radiol* 2003; **13**: 1559-1565

S- Editor Liu Y **L- Editor** Worthley DL **E- Editor** Lu W

胆と膵 Vol. 27 (1) p. 55~60, 2006

感染性膵壊死・膵膿瘍に対するEUSガイド下ドレナージ術*

今津博雄[1]・Salem Omar[2]・Stefan Seewald[2]
Nib Soehendra[2]・角谷宏[1]・田尻久雄[3]

要約：超音波内視鏡(EUS)の役割はCurvilinear型EUSの発達により，診断から治療へ転換しつつあり，Interventional EUSという言葉も使われるようになった。急性膵炎の合併症として生じる膵膿瘍・膵壊死に対する治療は手術療法が主流であるが，重篤な病態が基礎にあるため比較的高いmorbidity, mortalityが報告されている。手術療法に代わる非侵襲的な治療法として経皮的ドレナージ術，内視鏡的ドレナージ術が試みられてきたが，治療効果としては決して満足のいくものではなかった。本稿では，われわれHamburg Groupが行っているInterventional EUSを中心とした膵膿瘍・壊死に対する内視鏡的治療を紹介，解説する。

Key words：interventional EUS，膵膿瘍・壊死，ドレナージ

はじめに

1992年，Villmanら[1]が膵腫瘍に対し初めてEndoscopic ultrasonography-guided fine needle aspiration (EUS-FNA)を行って以来，この手技は欧米を中心に普及し，現在では消化器疾患のみならず，呼吸器疾患，血液疾患，泌尿器疾患など，さまざまな領域で日常的な外来診療として行われている。さらに，このEUS-FNAの手技は治療手技に応用され，経胃・十二指腸的膵仮性嚢胞ドレナージ術[2]，肝膿瘍ドレナージ術[3]，EUSガイド下薬剤注入療法[4,5]などが報告されるようになり，この領域はInterventional EUSと総称されるようになってきている。筆者と国立マレーシア大学のDr. Salem OmarはUniversity Hospital Hamburg-Eppendorf (UKE)においてEUS fellowとしてInterventional EUSのHands-on trainingを受けた（筆者は2003年10月から2004年9月まで。Dr. Omarは現在も研修中)。本稿において，われわれHamburg GroupがおこなっているInterventional EUSを用いた感染性膵壊死・膵膿瘍に対する治療法を中心に解説する。

II. 膵膿瘍・膵壊死の定義とConventional treatment

1992年，急性膵炎の臨床的分類システムを確立する目的で，国際シンポジウムがアトランタで開かれた。この分類はアトランタ分類[6]と呼ばれ，現在，膵炎を論じるときに世界で最も多く使われている分類である。それによると膵壊死とはびまん性あるいは巣状の膵実質壊死で，通常は膵周囲の脂肪壊死を伴うものと定義され，膵壊死に感染を伴った場合（感染性膵壊死）は伴わない場合(sterile)に比べ，3倍のMortalityリスクがあることが述べられている。膵膿瘍とは周囲を囲まれた腹腔内の膿貯留で，通常は膵に近接して存在し，膵壊死はないか，あってもわずかと定義されている。

感染性膵壊死・膵膿瘍とも急性膵炎，特に重症急性膵炎の経過中に発生する重篤な病態である。これらの病態に対して，すべての壊死組織と化膿組織を取り除くことが治療の最終目的であり，治療法として，現在，外科治療が主流であることは言うまでもない。

* EUS-guided Drainage for Pancreatic Abscess and Necrosis

1) 東京慈恵会医科大学内視鏡科（〒105-8461 港区西新橋3-25-8)
2) Department of Interdisciplinary Endoscopy, University Hospital Hamburg-Eppendorf
3) 東京慈恵会医科大学消化器・肝臓内科

International Association of Pancreatology (IAP) が2002年に出した急性膵炎に対する外科治療のガイドライン[7]では，①open Necrosectomy＋closed continous lavage，②open necrosectomy＋drainage＋re-laparotmy，③open necrosectomy＋open packing＋re-laparotomy が推奨されている。しかし，これらの手法ではLaparotomyを反復して行う場合が少なくなく，依然，手術療法には高いMortalityとMorbidityが報告されている[8~11]。

また，手術療法に代わる非侵襲的な治療法として，経皮的カテーテルドレナージや経皮的necrosectomyの報告がなされてきた[12~14]が，この多くは開腹術による追加治療を必要としている。現在のところ経皮的治療は炎症が限局した病態に対してのみ有効であるというのが一般的な知見である[7]。

III. 感染性膵壊死・膵膿瘍に対するEndoscopic treatment

1988年，Huibregtseら[15]により，初めて膵膿瘍に対する経乳頭的ドレナージ術が報告された。膵膿瘍2例に対し経乳頭的ドレナージ術を行い，十分なドレナージが得られたが，最終的には手術療法が行われた。その後，Venuら[16]により膵膿瘍に対する経乳頭的ドレナージ術の高い成功率が報告された。それによると外科治療が困難と判断された膵膿瘍15例のうち膵管と膵膿瘍が交通していた11例に対し，経乳頭的ドレナージ術を行い，8例(74%)が内視鏡治療のみで膵膿瘍が改善した。Venuらの方法は乳頭切開後，カテーテルを経乳頭的に膿瘍腔まで挿入し，生理食塩水で洗浄した後，10 Frのステントを留置するというもので，平均2.5回のERCP，平均110日の入院期間を要したとしている。

これに対し，Binmoellerら[17]は，1993年に初めて膵膿瘍に対し超音波内視鏡（EUS）ガイド下で経胃・十二指腸的ドレナージを行い，80%が内視鏡治療で改善したと報告した。その後も，少ない症例数ではあるが，EUSガイド下膵膿瘍ドレナージの有用性が報告された[18,19]。Parkら[20]はEUSを用いず，胃・十二指腸壁に膵膿瘍による圧排所見（bulging sign）のある症例9例11膵膿瘍に対し，経胃・十二指腸的に膵膿瘍をkneedle knifeを用いて穿刺，洗浄を行い，ステントもしくは経鼻膿瘍ドレナージチューブを膿瘍腔に留置したところ91%で膿瘍の消失が得られ，1例で出血により手術療法を行ったと報告した。Baronら[21]は慢性仮性嚢胞64例，急性仮性嚢胞31例，膵壊死43例に経胃・十二指腸的ドレナージ，経乳頭的ドレナージと洗浄を行ったところ，慢性仮性嚢胞が急性仮性嚢胞（膵膿瘍を含む），膵壊死に比べ有意にその消失率が高く(92% vs. 74% p=0.02, 72% p=0.006)，合併症の発生率と治癒後の再発率は膵壊死で有意に高かった（37%，29%）としている。これらの結果から，膵膿瘍・壊死に対して内視鏡的ドレナージは有用な治療法であることが窺えるが，手術療法に移行する症例も少なくなく，とりわけ膵壊死ではその傾向が強いと思われる。その原因として一般にカテーテルを用いたドレナージだけでは化膿・壊死組織の除去が不十分であることや，膵管とのfistulaの存在が挙げられる。

UKEではこれらの内視鏡治療の問題点を克服すべく，1997年よりInterventional EUSを中心に大きく3つの内視鏡治療を組み合わせ，感染性膵壊死・膿瘍の治療を行い，良好な治療成績を得ている。われわれはこの手法を“Endoscopic triple approach”と呼んでいる。

以下にEndoscopic triple approachの手技について解説する。

IV. Endoscopic Triple Approach

この手技は大きく次の3つのステップからなる。

1．第1ステップ：ERP（内視鏡的逆行性膵管造影）下の経乳頭的ドレナージ＋EUSガイド下経胃・十二指腸的ドレナージとcystogastrostomaあるいはcystoduodenostomaのバルーン拡張

まず始めにERPを行い膵管の評価を行う。そして膵管と壊死部あるいは膿瘍腔に交通(fistula)が認められた場合に経乳頭的ドレナージ術を行う。経乳頭的ドレナージの方法であるが，まず，膵管へのカニュレーションにはダブルルーメンのパピロトームを用いて0.032-inchラジフォーカスガイドワイヤーを先行させてカニュレーションを行う（これは日本では馴染みの少ない，欧米でよく行われる挿管法で，筆者も慣れるまで時間を要した)。次に，パピロトームをfistulaまで誘導したのち，ガイドワイヤーをDispo-Medica 0.035-inchガイドワイヤー（日本ではジャグワイヤーにあたる)に交換し，7 Frテフロン製Nasopancreatic catheter（NPC：H. C. Grosse）を挿入し，経乳頭的ドレナージは終了する。この際，膵管狭窄がみられた場合はBrushing cytologyや経過により膵管ステント留置を行う。

ERPによる膵管の評価後，経乳頭的ドレナージを行った症例も含めて，全例にEUSガイド下で経胃・十

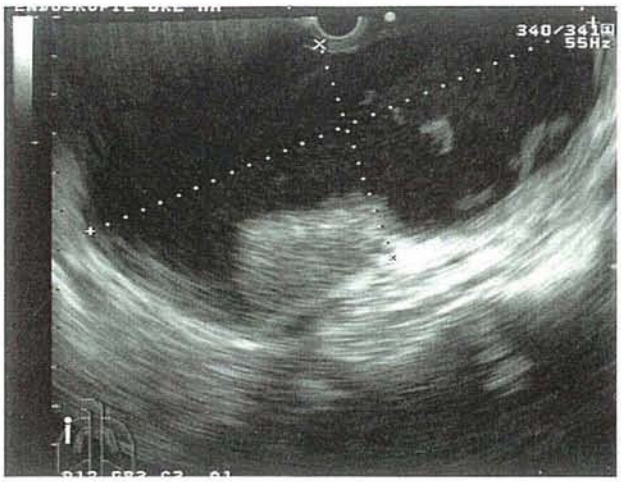

図 1　膵膿瘍の EUS 像

図 2　第 1 ステップ
EUS ガイド下に 6Fr Teflon シースを被せた 22G GIP needle で膿瘍腔を穿刺する。

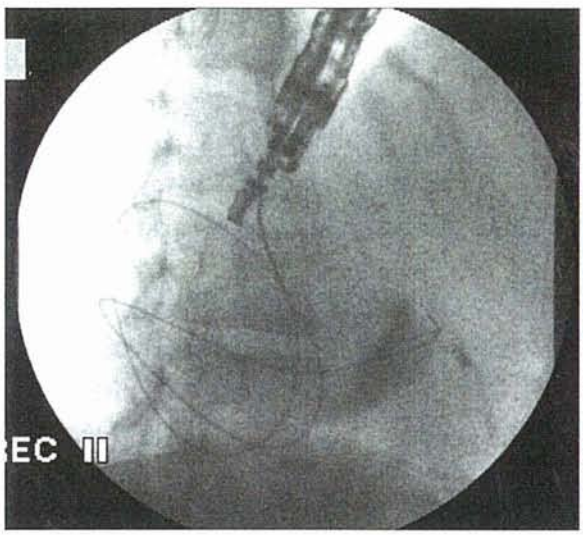

図 3　第 1 ステップ
ドレナージチューブを挿入する前段階として，透視下でガイドワイヤーを膿瘍腔内に挿入する。

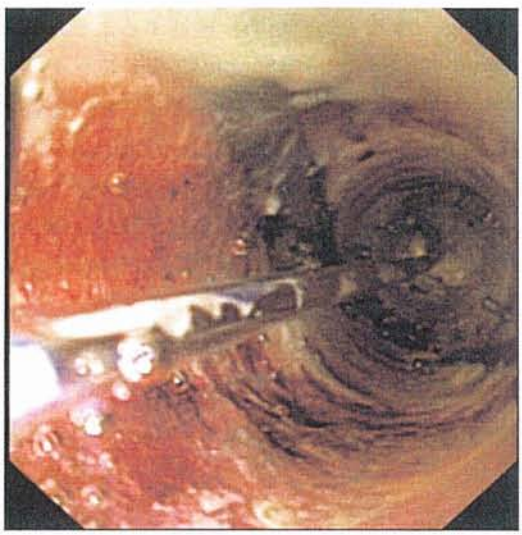

図 4　第 1 ステップ
第 2 ステップの前段階として拡張バルーンにより，穿刺孔を拡張する。

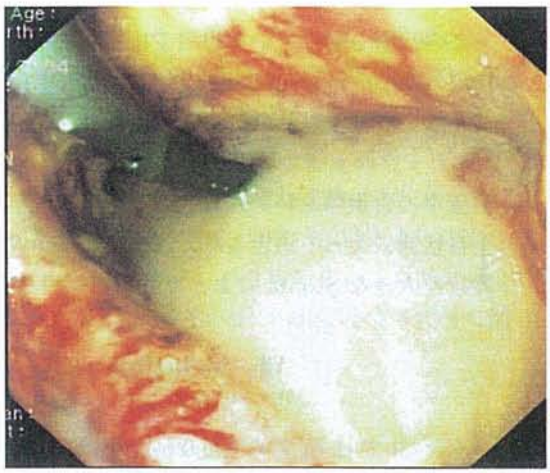

図 5　第 2 ステップ
Cystogastrostoma から膿瘍腔に内視鏡を挿入する。膿瘍腔の内視鏡像では膿瘍・壊死組織がみられ，ドレナージチューブが挿入されている。この位置から内視鏡の suction 機能あるいはバスケットを用いて necrosectomy を行う。

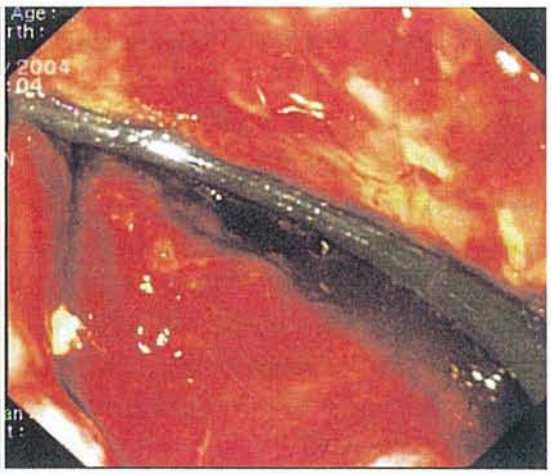

図 6　第 2 ステップ
Necrosectomy を反復したことで膿瘍腔は縮小し，赤色の肉芽組織が出現している。

二指腸的ドレナージを行う。EUSスコープにはCurvilinear型のOlympus Medical System社製GF-UCT 140-AL5を，プロセッサーにはアロカ社製SSD 5000 US Systemを用いている。

まず病変を胃もしくは十二指腸から描出し（図1），color-flow Dopplerで穿刺ルートに血管が存在しないことを確認した後，6 Frのテフロンシース（H. C. Grosse）を被せた22ゲージGIP needle（Medi-Globe）で壊死・膿瘍腔をEUSガイド下に穿刺する（図2）。その後，シースを残してGIP needleを抜去し，0.035 inch Tracer Wire Guide（Wilson-Cook）を挿入する（図3）。次に，消化管用の拡張バルーン（Microvasive Endoscopy）を挿入，穿刺孔を拡張する（図4）。バルーン拡張は理論的には10 mmから20 mmまで拡張が可能であるが，穿孔予防のため，後述するように拡張は一期的に行わないで，段階的に行う。ドレナージチューブの挿入が可能な拡張孔が得られた後，拡張バルーンを抜去，7 Fr Nasocyctic Teflon Catheter（H. C. Grosse）と10 Fr 5 cm double-pigtail stent（H. C. Grosse）を壊死・膿瘍腔に挿入し，第1ステップの手技は終了である。また，この7 Fr Nasocyctic Teflon Catheterを注入ルート，10 Fr 5 cm double-pigtail stentを排出ルートにして，1日1500 m*l*の生理食塩水による洗浄を行う。

2．第2ステップ：内視鏡的Necrosectomyと洗浄

第2ステップで治療を終了しては今までの報告どおり，すべての壊死組織を除去することは不可能で，不十分に終わってしまう。UKEではほぼ毎日，ドレナージチューブの挿入孔をバルーンで段階的に拡張し，十分な拡張孔が得られた後，内視鏡スコープそのものを壊死・膿瘍腔に挿入し，内視鏡下でNecrosectomyを行う。

最初は小児用スコープ（GIF XP 160, 240, Olympus）とバスケットを用いて，後に処置用スコープ（GIF XT 30, Olympus）のSuction機能を用いてNecrosectomyを行う（図5）。Necrosectomyはすべての壊死組織が除去され，新しい肉芽組織が出現（図6）してくるまで，毎日行う。Nasocystic Teflon Catheterは壊死・膿瘍腔にスコープの挿入が可能になった時点で抜去し，内視鏡下のみで洗浄を行う。これで第2ステップの手技は終了である。

3．第3ステップ：cyanoacrylateによるfistula sealing

第2，第2ステップの治療が終了したら，ERPを再度行う。膵管と縮小した壊死・膿瘍腔にfistulaは第1，第2ステップの治療で自然に閉鎖する場合もあるが，依然，fistulaが存在する場合はERP下でfistulaにN-butyl-2-cyanoacrylate（Histoacryl）0.5 m*l*とLipiodol 0.3 m*l*の混合液を注入し，fisutula sealingを行う[22]。これで第3ステップの手技は終了である。

V. Endoscopic triple approachの適応

膵壊死・膿瘍の治療の主流は外科治療であることは先に述べた。現在のところUKEでは病態が重篤で全身状態が不良のため，あるいは重篤な心疾患などを合併し，緊急手術に耐えられないと判断された症例にのみ，このEndoscopic triple approachを行っている。

VI. Endoscopic triple approachの成績

UKEのEndoscopic triple approachの治療成績は2005年にDr. Seewaldによって報告された[23]。要約すると感染性膵壊死5例，膵膿瘍8例に対し，Endoscopic triple approachを行い，13例が内視鏡治療のみで治癒し，傍結腸腔に壊死が波及していた1例で外科治療が追加されたという結果であった。バルーン拡張とNecrosectomyの回数は中央値でそれぞれ3回，7回で，手技による合併症は軽度の出血を4例に認めたのみであった。ドレナージを開始してからの入院期間は中央値で32日間であり，経過中（観察期間の中央値：9.5ヵ月）に2例で仮性嚢胞の発達を認め，また1例で膵癌を合併していたため待機的に外科治療が追加された。結局，約3分の2の症例で外科治療が回避できたが，少なくとも全例で緊急手術を避けることができたと言えよう。

この治療を受けている患者で出室可能な場合は，ほぼ毎日Necrosectomyと洗浄のため内視鏡室にやってくる（不可能な場合はICUで行う）。そして，特に第1ステップの治療で状態が劇的に改善していく。また，治療中の食事開始時期は，基本的に患者の膵炎の程度，全身状態によって決定され，Necrosectomyのために開けた大きなStomaによって制限は受けない。

VII. Sedation

ドイツでは通常のGastroscopyからEndoscopic triple approachまで，すべての検査・治療手技をPropofolによるSedaition下で行っている。もちろん，内視鏡室に麻酔科医などいない。Propofolは速効性で覚醒もきわめて早く，内視鏡時のDeep sedation

に用いる薬剤としては，モニタリングを適切に行っていれば非常に安全かつ効果的な薬剤である。筆者はUKEで実際の術者としてあるいは，介助者として1年間で1200例の診断的EUSとInterventional EUSを経験したが，Propofolを用いたSedationによるトラブルはまったく経験していない。わが国では内視教室でPropofolを使用することは保険診療上できない。今後，積極的な内視鏡治療を行っていく上で，ぜひとも必要な薬剤であり，保険診療ならびに制度上の問題の解決が望まれる。

おわりに

Curvilinear EUSが開発され，この機種は欧米を中心に普及し，Interventional EUSも欧米を中心に発展してきた。Radial EUSが普及しているわが国が，この領域で遅れを取っていることは否めない。その理由として，Curvilinear EUSがRadialより安価であったため欧米で普及した，あるいは，わが国ではすでにRdial EUSを導入している施設が多く，さらにCurvilinear EUSを導入して，2台のシステムを同時に持つことは経済的に困難であり，そのためCurvilinear EUSは普及しなかったと言われている。しかしながら，EUSおよびEUS-FNAはCT，PET等の他の画像診断より，臓器によっては診断能が優れているというエビデンスがある[24~26]。また安全なSedationにより，もはや内視鏡検査はCT等と比べ，侵襲的検査であるという認識がなくなったため，EUS-FNAを中心としたInterventional EUSが欧米で普及・発展してきたものと考られる。今後，わが国においてもInterventinal EUSの発展を期待したい。

参考文献

1) Vilmann P, Jacobsen GK, Henriksen FW, et al.：Endoscopic ultrasonography with guided fine needle aspiration biopsy in pancreatic disease. Gastrointest Endosc **38**：172-173, 1992.
2) Binmoeller KF, Soehendra N：Endoscopic ultrasonography in the diagnosis and treatment of pancreatic pseudocyst. Gastrointest Endosc Clin N Am **5**：805-816：1995.
3) Seewald S, Imazu H, Omar S, et al.：EUS-guided drainage of hepatic abscess. Gastrointest Endosc **61**：495-498, 2005.
4) Chang KJ, Nguyen PT, Thompson JA, et al.：Phase I clinical trial of allogeneic mixed lymphocyte culture (cytoimplant) delivered by endoscopic ultrasound-guided fine-needle injection in patients with advanced pancreatic carcinoma. Cancer **88**：1325-1335, 2000.
5) Chang KJ, Senzer N, Chung T：A novel gene transfer therapy against pancreatic cancer (TNFerade), delivered by endoscopic ultrasound (EUS) and percutaneous guided fine-needle injection (FNI). Gastrointest Endosc **59**：AB92, 2004.
6) Bradley E：A clinically based classification system for acute pancreatitis. Arch Surg **128**：586-590, 1993.
7) Uhl W, Warshaw A, Imrie C, et al.：IAP guidelines for the surgical management of acute pancreatitis. Pancretol **2**：565-573, 2002.
8) Fernandez-del Castillo C, Rattner DW, Makary MA, et al.：Debridement and closed packing for the treatment of necrotizing pancreatitis. Ann Surg **228**：676-684, 1998.
9) Hartwig W, Werner J, Muller CA, et al.：Surgical management of severe pancreatitis including serile necrosis. J Hepatobiliary Pancreat Surg **9**：429-435, 2002.
10) Branum G, Galloway J, Hirchowitz W, et al.：Pancreatic necrosis：results of necrosectmy, packing and ultimate closure over drains. Ann Surg **227**：870-677, 1998.
11) Tisiotos GC, Luque-de Leon E, Soreide JA, et al.：Managementof necrotizing pancreatitis by repeated operative necrosectomy using a zipper technique. Am J Surg **175**：91-98, 1998.
12) Cater CR, Mckay CJ, Imrie CW, et al.：Percutaneous necrosectomy and sinus tract endoscopy in the management of infected pancreatic necrosis：An initial experience. Ann Surg **232**：175-180, 2000.
13) vanSonnenberg E, Wittich GR, Chon KS, et al.：Percutaneous radiologic drainage of pancreatic abscess. Am J Roentgenol **168**：979-984, 1997.
14) vanSonnenberg E, Wittich GR, Goodacre BW, et al.：Percutaneous abscess drainage：update. World J Surg **25**：362-369；discussion 370-372, 2001.
15) Huibregtse K, Schneider B, Vriji AA, et al.：Endoscopic pancreatic drainage in chronic pancreatitis. Gastrointest Endosc **34**：9-15, 1988.
16) Venu RP, Brown RD, Marrero JA, et al.：Endoscpic transpapillary drainage of pancreatic abscess：technique and results. Gastrointest Endosc **51**：391-395, 2000.
17) Binmoeller KF, Walter A, Seifert H, et al.：Endoscopic therapy for pancreatic abscess. Gastrointest Endosc **39**：AB308, 1993.
18) Seifert H, Dietrich C, Schmitt T, et al.：Endoscopic ultrasound-guided one-step transmural drainage of cystic abdominal lesions with a large-channel echo endoscope. Endosc **32**：255-259, 2000.

19) Giovannini M, Pesenti C, Rolland AL, et al. : Endoscopic ultrasound-guided drainage of pancreatic pseudocyst or pancreatic abscess using a therapeutic echo endoscope. Endosc **33** : 473-477, 2001.
20) Park JJ, Kim SS, Koo YS, et al. : Deffinitive treatment of pancreatic abscess by endoscopic transmural drainage. Gastrointest Endosc **55** : 256-262, 2002.
21) Baron TH, Harewood GC, Morgan DE, et al. : Outocome differences after endoscopic drainage of pancreatic necrosis, acute pancreatic pseudocysts, and chronic pancreatic pseudocysts. Gastrointest Endosc **56** : 7-17, 2002.
22) Seewald S, Brand B, Groth S, et al. : Endoscopic sealing of pancreatic fistula by using N-butyl-2-cyanoacrylate. Gastrointest Endosc **59** : 463-470, 2004.
23) Seewald S, Groth S, Omar S, Imazu H, et al. : Aggressive endoscopic therapy for pancreatic necrosis and abscess : a new safe and effective treatment algorithm. Gastrointest Endosc **62** : 92-100, 2005.
24) Tierney WM, Francis K, Eckhauser F, et al. : The accuracy of EUS and helical CT in assessment of vascular invasion by peripapillary tumor. Gastrointest Endosc **53** : 182-188, 2001.
25) Mertz HR, Sechopolous P, Delbeke D, et al. : EUS, PET and CT scanning for evaluation of pancreatic adenocarcinoma. Gastrointest Endosc **52** : 367-371, 2000.
26) Fritscher-Ravens A, SriramPV, Krause C, et al. : Detection of pancreatic metastasis by EUS-guided fine needle aspiration. Gastrointest Endosc **53** : 65-70, 2001.

*　　*　　*

産婦人科の実際 第55巻 第13号 (2006年12月1日 発行)

特集 卵巣癌の新しい予後因子とバイオマーカー

プロテインチップによる新しい予後因子やバイオマーカー探索

山田恭輔　上田　和　石塚康夫
岡本愛光　安田　允　田中忠夫

金原出版株式会社

特集 卵巣癌の新しい予後因子とバイオマーカー

プロテインチップによる新しい予後因子やバイオマーカー探索

山田恭輔* 上田 和* 石塚康夫*
岡本愛光* 安田 允* 田中忠夫*

ゲノム医科学の進歩にともない，タンパク質の全体（プロテオーム）を大規模に解析するプロテオミクス研究が注目されている。近年，がん研究において高感度のプロテオミクス技術を用いた新しい予後因子やバイオマーカー探索が行われるようになった。卵巣癌は化学療法の進歩により予後が改善されつつあるが，進行がんや再発がんの予後はきわめて不良である。早期発見やオーダーメイド医療を目指したプロテオミクス研究の成果に期待がかかり，実際に臨床検体を用いた解析が進められている。

はじめに

ポストゲノム時代の到来とともに，ゲノム医科学によるがん研究の分野においてはDNAマイクロアレイを用いた遺伝子の増幅・欠失やcDNAマイクロアレイを用いた遺伝子発現の検索など網羅性，包括性を目指す大規模解析の技術が著しく進歩した。卵巣癌研究においても遺伝子レベルでの網羅的データ解析の蓄積がなされてきた。さらに近年，ゲノム情報の最終的な表現型であるタンパク質の全体（プロテオーム）を大規模に解析するプロテオミクス研究が始まっている。プロテオミクスの考え方は，遺伝子レベルでの網羅的解析から自然の流れで生まれたといってよいのかもしれない。

プロテオミクスは，遺伝子の発現情報をタンパク質のレベルで定量的に解析する発現プロテオミクスと，相互作用を基礎にしてタンパク質機能を理解することを目的にした機能プロテオミクスに大別される[1]。近年，さまざまな癌腫において高感度のプロテオーム技術を用いた研究が行われているが[2]，卵巣癌においては発現プロファイル解析が始まったばかりの段階といえる。遺伝子レベルの研究においても，その機能を理解しなければ臨床応用には結びつかないのは当然であり，ましては無数に存在するタンパク質の包括的理解などゴールが遠いとする見解もあるが，バイオマーカー探索という観点からは期待できる研究成果も出ている。

*Kyosuke YAMADA, Kazu UEDA, Yasuo ISHIZUKA, Aikou OKAMOTO, Makoto YASUDA, Tadao TANAKA
東京慈恵会医科大学産婦人科
〒105-0005 東京都港区西新橋3-19-18

I. がん研究におけるゲノミクスとプロテオミクス

マイクロアレイなどを用いた網羅的な遺伝子の情報解析にはどのような意義があるのであろうか。mRNAを対象とするトランスクリプトームのレベルで考えれば，がん組織でのみ特異的に発現している遺伝子ががん遺伝子の候補と考えられ，逆に発現が抑えられている遺伝子ががん抑制遺伝子の候補と考えられ，網羅的

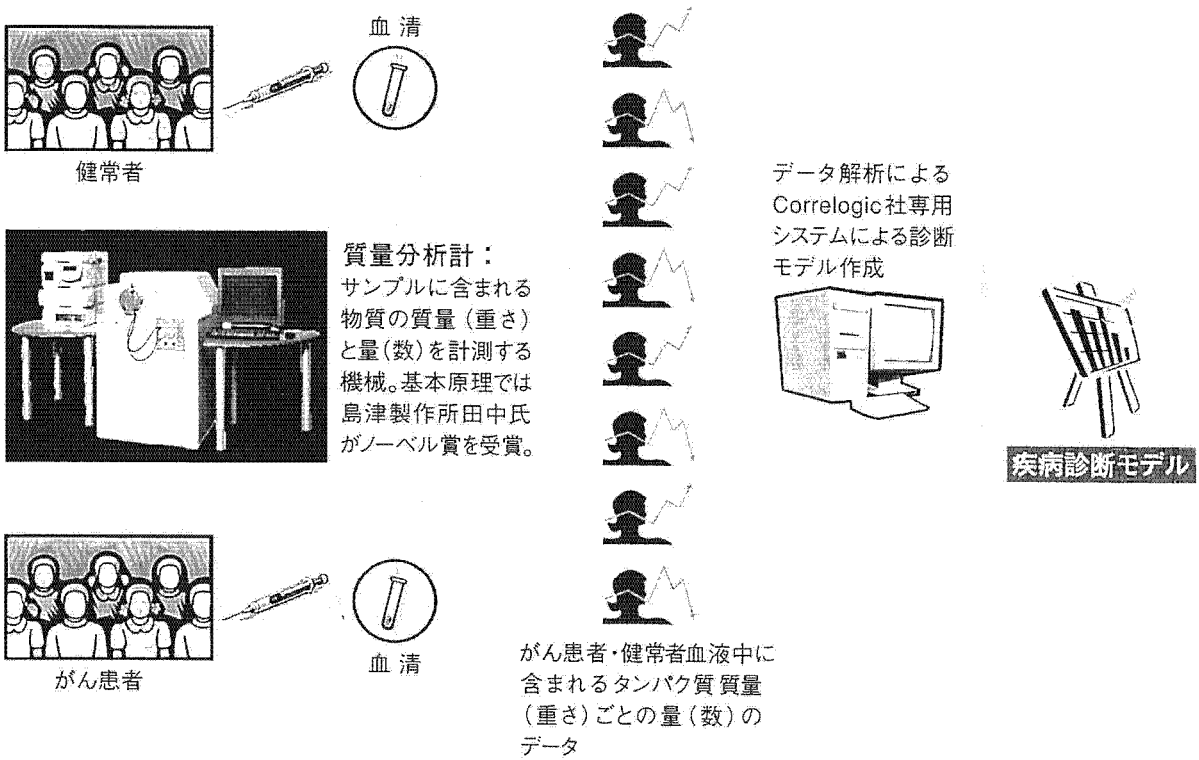

図1　診断モデル作製のプロセス

検索から新しい遺伝子の発見や発がん・進展メカニズムの解明に有用な情報を得ることができる。しかし，mRNAは遺伝情報をタンパク質に変換するためのもので，その動態が必ずしも細胞内タンパク質発現と相関しない，リン酸化などタンパク質の修飾についての情報が得られないなどの問題点がある。現在のプロテオミクス技術は網羅性，再現性，定量性など総合的に判断するとマイクロアレイに比し確立されたものではないが，タンパク質の大規模解析はゲノミクスからの情報と連携し今後の研究戦略として不可欠と考えられる。

II. 新しいバイオマーカー探索

CA125は現在卵巣癌マーカーとして広く使用されているが，進行がんにおいては約80%の患者で高値を示すものの，I期がんでは50～60%の患者でのみ陽性を示すにとどまる。CA125はシングルマーカーとしては正の予測価（positive predictive value：有病かつ検査結果が陽性のものと検査結果が陽性なものの人数の比）は10%以下とされる。また，欧米に比べわが国において発生頻度が高いとされる明細胞腺癌は，腫瘍マーカーの陽性率が低いという問題点が指摘されている。

現在プロテオミクスによる卵巣癌の新しいバイオマーカー探索が進められている。従来の腫瘍マーカーは，特定のタンパク質など血清中の特異抗原の有無に限定して検査を行うため診断精度に限界があったのに対し，プロテオミクスによる診断は複数物質の量を複合的に解析するため，より精度の高い診断が可能となる[3]。プロテインチップを用いることで多数のタンパク質群を同時に検索できることから，単にタンパク質発現の有無だけではなくパターン認識（クラス分け）による解析が可能となる。実際には，プロテインチップにて網羅的解析ができる対象タンパク質は低分子量のもので，分子量20 kDを超えるタンパク質のプロテオーム技術としては二次元電気泳動を超えるものは登場していない[4]。プロテオミクスと称する研究の中

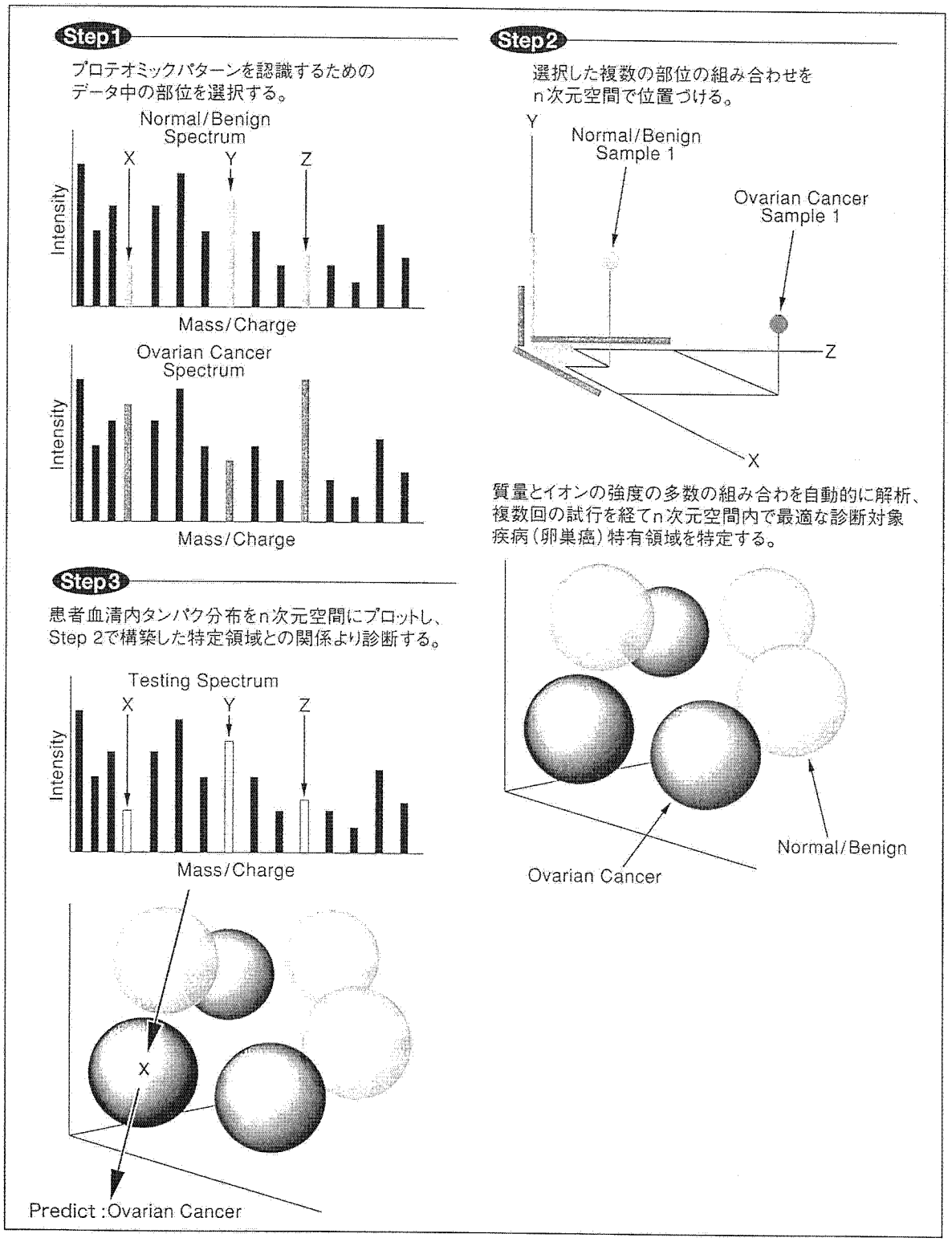

図2　診断モデルの構築と解析（Proteome Quest®）

にも，機能をもったタンパク質群を見ているのではなく，低分子の代謝産物を見ているにすぎないものもある。しかし，複数物質の発現をパターン認識しようとする試みは，既存の腫瘍マーカーよりも感受性，特異性ともにすぐれたマーカーを探索することにつながると考えられる。

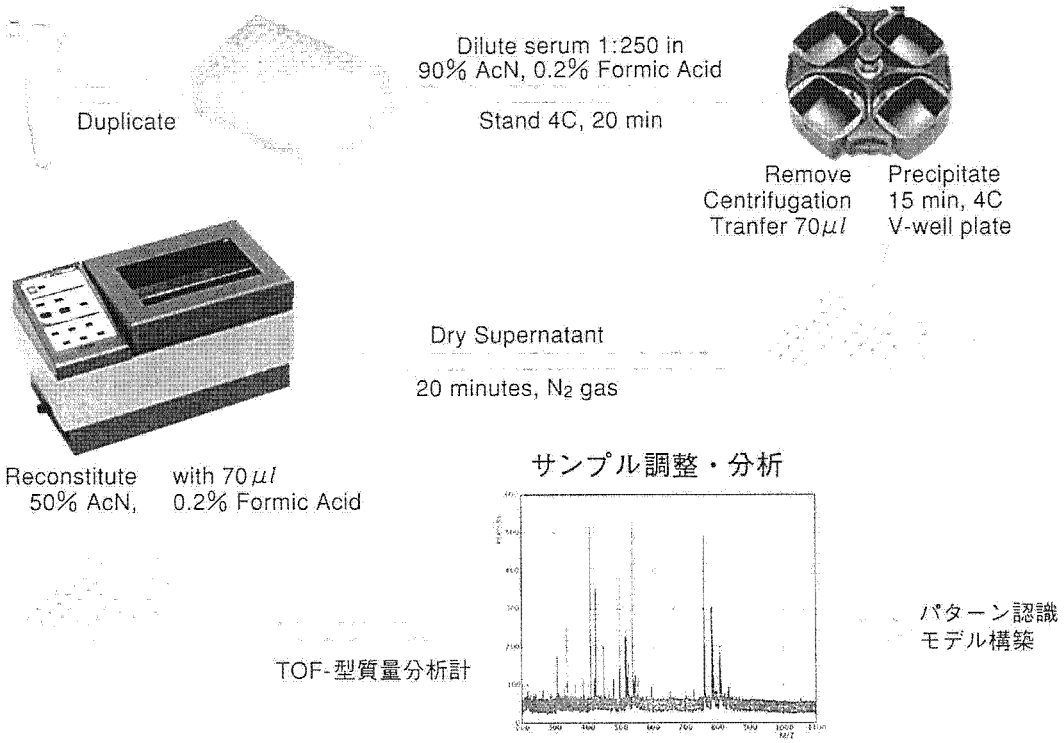

図３　血清診断における検体調整法

III. 新しい予後因子の探索

卵巣癌の新しい予後因子の探索につながるアプローチとしては，ある事象に関係のあるタンパク質群に注目し，プロテインチップによりその候補を検索することである。この考え方は，遺伝子レベルでの解析ではすでに多くの報告がある。例えば，パクリタキセル耐性のあるがんと薬剤感受性の癌を比較し薬剤耐性に関連する遺伝子群をクラス分けする[5]，すでに確立している病理学的な診断とマイクロアレイの結果のパターンを照合し，マイクロアレイの結果から病理診断を裏付けようとするものなどである。また，マイクロアレイの結果から，新たにクラス分けをしようとする方法があり，同じ組織型・進行期であっても予後良好群と不良群の遺伝子発現の違いをパターンの差異から読み取ろうとするものである。このような考え方に基づき，がんの悪性形質を裏付けるタンパク質群を同定あるいはクラス分けしようとするプロテオミクス研究は，新しい予後因子の探索に有用と考えられる[6]。

IV. SELDI-TOF MS

近年，より高感度のプロテオーム技術である SELDI-TOF MS（surface enhanced laser desorption/ionization time of flight mass spectrometry）が，卵巣癌，乳癌，膵癌，膀胱癌，前立腺癌などの研究に応用されている。SELDI-TOF MS とは，タンパク質あるいはペプチドをプロテインチップ上に添加し，イオン化させて発現パターンを観察する技術である。検出系に質量分析器を用いているので感度が高いこと，主に分子量 20 kD 以下のタンパク質あるいはペプチドが解析の対象になる。SELDI-TOF 質量分析器については Ciphergen 社（Freemont, USA）の資料より検出の要点を以下に示す。プロテインチップで捕捉されたタンパク質はパルスレーザーの照射によってチップ表面から「脱離」し，イオン化されて固相から飛行する。イオン化されたタンパク質の飛行時間が質量分析